

Spectrum of π electrons in bilayer graphene nanoribbons and nanotubes: an analytical approach

J. Ruseckas* and G. Juzeliūnas

Institute of Theoretical Physics and Astronomy, Vilnius University A. Goštauto 12, LT-01108 Vilnius, Lithuania

I. V. Zozoulenko

Solid State Electronics, ITN, Linköping University, 601 74 Norköping, Sweden

We present an analytical description of π electrons of a finite size bilayer graphene within a framework of the tight-binding model. The bilayered structures considered here are characterized by a rectangular geometry and have a finite size in one or both directions with armchair- and zigzag-shaped edges. We provide an exact analytical description of the spectrum of π electrons in the zigzag and armchair bilayer graphene nanoribbons and nanotubes. We analyze the dispersion relations, the density of states, and the conductance quantization.

PACS numbers: 73.22.Pr

I. INTRODUCTION

Since its isolation in 2004, graphene—a single sheet of carbon atoms arranged in a honeycomb lattice—has attracted an enormous attention because of its highly unusual electronic and transport properties that are strikingly different from those of conventional semiconductor-based two-dimensional electronic systems (for a review see Refs. 1–4). It has been immediately realized the significance and the potential impact of this new material for electronics. This far, it has been demonstrated that the graphene has the highest carrier mobility at room temperature in comparison to any known material⁵. However, graphene is a semimetal with no gap and zero density of states at the Fermi energy. This makes it difficult to utilize it in electronic devices such as field effect transistor (FET) requiring a large on/off current ratio. The energy gap can be opened in a bilayer graphene by applying a gate voltage between the layers⁶. This gate-induced bandgap was demonstrated by Oostinga *et al.*⁷, and the on/off current ratio of around 100 at room temperature for a dual-gate bilayer graphene FET was reported by the IBM⁸.

Another way to introduce the gap is to pattern graphene into nanoribbons^{9,10}. The conductance of graphene nanoribbons (GNRs) with lithographically etched edges indeed revealed the gap in the transport measurements^{11,12}. This gap has been subsequently understood as the edge-disorder-induced transport gap^{13–15} rather than the intrinsic energy gap expected in ideal GNRs due to the confinement⁹ or electron interactions and edge effects¹⁰. During last years the great progress has been achieved in fabrication and patterning of the GNRs with ultrasmooth and/or atomically controlled edges. This includes e.g. a controlled formation of edges by Joule heating¹⁶, unzipping carbon nanotubes to form nanoribbons¹⁷, chemical route to produce nanoribbons with ultrasmooth edges¹⁸ and atomically precise bottom-up fabrication of GNRs¹⁹. All these advances in nanoribbons fabrication will hopefully enable not before long the electronic measurement in near-perfect nanoribbons free from the edge or bulk disorder defects.

An important insight into electronic properties of graphene and GNRs can be obtained from exact analytical approaches. The analytic calculations for the electronic structure of the GNRs have been reported in Refs. 20–24. The electronic structure of the bilayer graphene was addressed in Refs. 25–29 where the analytical results were presented (both exact and perturbative). We are not however aware of analytical treatment of bilayer GNRs (Note that a numerical study of the magnetobandstructure of the GNRs was reported in Ref. 30 and 31, and the analytical and numerical treatment of the edge states in the bi- and N-layer graphene and GNRs was presented in Refs. 29 and 32). The purpose of the present study is to provide an exact analytical description of the spectrum of π electrons in the zigzag and armchair bilayer nanoribbons and nanotubes including the dispersion relations, the density of states, and the conductance quantization.

The paper is organized as follows: In order to illustrate our method, in Sec. II we present known analytical results for a simpler system, monolayer graphene of the finite size. Subsequently in Sec. III we derive the main analytical expressions for the energy spectrum of finite-size structures of bilayer graphene. These expressions are used in Sec. IV to analyze the energy spectrum of various bilayer graphene structures near the Fermi energy. Finally, Sec. V summarizes our findings.

II. SINGLE LAYER GRAPHENE

Analytical expressions for the π electron spectrum in GNRs and graphene nanotubes (GNTs), based on tight-binding model, were provided in Ref. 23. In this section we will rederive the same expressions in an analytically simpler way. Our method more clearly shows the connection between solutions for the infinite sheet of graphene and for the finite-size sheet. In addition, simpler method will allow us to derive later on analytical expressions of the π electron spectrum for more complex systems, bilayer GNRs and GNTs.

A. Electron spectrum in infinite sheet of graphene

First we will consider π electron spectrum in an infinite sheet of graphene. Hexagonal structure of graphene is shown in Fig 1a. The structure of the graphene can be viewed as a hexagonal lattice with a basis of two atoms per unit cell. The Cartesian components of the lattice vectors \mathbf{a}_1 and \mathbf{a}_2 are $a(3/2, \sqrt{3}/2)$ and $a(3/2, -\sqrt{3}/2)$, respectively. Here $a \approx 1.42 \text{ \AA}$ is the carbon-carbon distance¹. The three nearest-neighbor vectors are given by $\boldsymbol{\delta}_1 = a(1/2, \sqrt{3}/2)$, $\boldsymbol{\delta}_2 = a(1/2, -\sqrt{3}/2)$, and $\boldsymbol{\delta}_3 = a(-1, 0)$. The tight-binding Hamiltonian for electrons in graphene has the form

$$H_{\text{gr}} = -t \sum_{\langle i,j \rangle} (a_i^\dagger b_j + b_j^\dagger a_i), \quad (1)$$

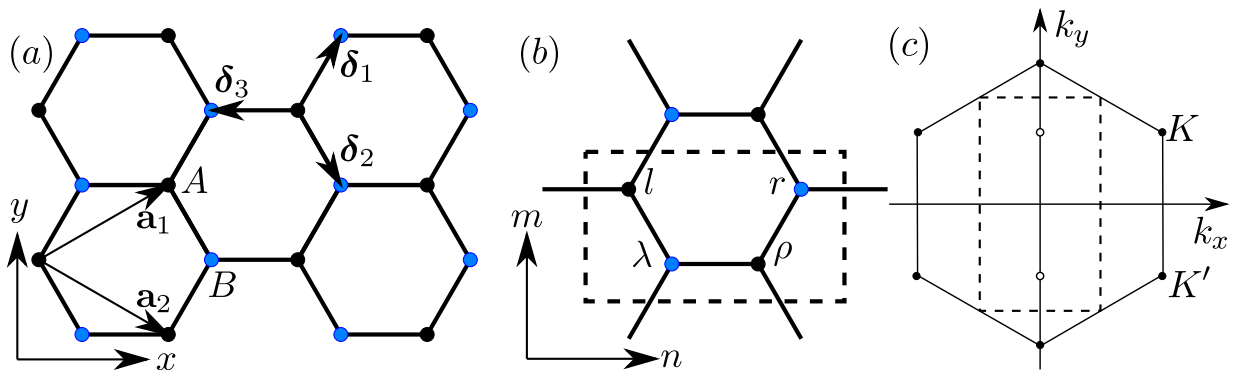


FIG. 1. (Color online) (a) Honeycomb lattice structure of graphene, made out of two interpenetrating triangular lattices. \mathbf{a}_1 and \mathbf{a}_2 are the lattice unit vectors, and $\boldsymbol{\delta}_i$, $i = 1, 2, 3$ are the nearest-neighbor vectors. (b) Indication of labels of carbon atoms in the rectangular unit cell. (c) Brillouin zones for hexagonal unit cell (solid hexagon) and rectangular unit cell (dashed rectangle). The Dirac points are indicated by solid circles for the hexagonal unit cell and hollow circles for the rectangular unit cell.

where the operators a_i and b_i annihilate an electron on sublattice A at site \mathbf{R}_i^A and on sublattice B at site \mathbf{R}_i^B , respectively. The parameter t is the nearest-neighbor hopping energy ($t \approx 2.8$ eV). From now on we will write all energies in the units of the hopping integral t , therefore we will set $t = 1$. Let us label the elementary cells of the lattice with two numbers p and q . Then the atoms in the sublattices A and B are positioned at $\mathbf{R}_{p,q}^A = p\mathbf{a}_1 + q\mathbf{a}_2$ and $\mathbf{R}_{p,q}^B = \boldsymbol{\delta}_1 + p\mathbf{a}_1 + q\mathbf{a}_2$, respectively.

The π electron wave function satisfies the Schrödinger equation,

$$H\Psi = E\Psi. \quad (2)$$

We search for the eigenvectors of the Hamiltonian (1) in the form of the plane waves (Bloch states) by taking the probability amplitudes to find an atom in the sites $\mathbf{R}_{p,q}^A$ and $\mathbf{R}_{p,q}^B$ of the sublattices A and B as

$$\psi_{p,q}^A = c^A e^{i\mathbf{k}\cdot\mathbf{R}_{p,q}^A}, \quad \psi_{p,q}^B = c^B e^{i\mathbf{k}\cdot\mathbf{R}_{p,q}^B}. \quad (3)$$

Thus Eq. (2) yields the eigenvalue equations for the coefficients c^A and c^B

$$-Ec^A = c^B \tilde{\phi}(\mathbf{k}), \quad (4)$$

$$-Ec^B = c^A \tilde{\phi}(-\mathbf{k}), \quad (5)$$

where

$$\tilde{\phi}(\mathbf{k}) \equiv e^{i\mathbf{k}\cdot\boldsymbol{\delta}_1} + e^{i\mathbf{k}\cdot\boldsymbol{\delta}_2} + e^{i\mathbf{k}\cdot\boldsymbol{\delta}_3}. \quad (6)$$

From Eqs. (4) and (5) we get the eigenenergies and the corresponding coefficients determining the eigenvectors

$$E(\mathbf{k}) = s_1 |\tilde{\phi}(\mathbf{k})|, \quad c^A = -\frac{\tilde{\phi}(\mathbf{k})}{E(\mathbf{k})}, \quad c^B = 1, \quad (7)$$

where $s_1 = \pm 1$. In the anticipation of the rectangular geometry we introduce dimensionless Cartesian components of the wave vector

$$\kappa = 3ak_x, \quad \xi = \sqrt{3}ak_y \quad (8)$$

instead of the wave vector components k_x and k_y . Then using the coordinates of the vectors $\boldsymbol{\delta}_j$ we have

$$\tilde{\phi}(\mathbf{k}) = e^{-i\frac{\kappa}{3}} + 2e^{i\frac{\kappa}{6}} \cos\left(\frac{\xi}{2}\right) \quad (9)$$

and the expression for the eigenenergies becomes¹

$$E(\mathbf{k}) = s_1 \sqrt{1 + 4 \cos^2\left(\frac{\xi}{2}\right) + 4 \cos\left(\frac{\xi}{2}\right) \cos\left(\frac{\kappa}{2}\right)}. \quad (10)$$

For satisfying boundary conditions it is useful to adopt a larger unit cell characterized the same geometry as the whole sheet of graphene. Since we are interested in configurations of the graphene with rectangular geometry, we will use a rectangular unit cell, as it has been done in Ref. 23. Such unit cell has four atoms labeled with symbols l , λ , ρ , r , as it is shown in Fig. 1b. The atoms with labels l and ρ belong to the sublattice A , the atoms with labels λ and r belong to the sublattice B . The position of the unit cell is indicated with two numbers n and m . The first Brillouin zone corresponding to the rectangular unit cell contains the values of the wave vectors κ , ξ in the intervals $-\pi \leq \kappa < \pi$, $-\pi \leq \xi < \pi$. We search for the eigenvectors having the form of plane waves,

$$\psi_{m,n,\alpha} = c_\alpha e^{i\xi m + i\kappa n}, \quad (11)$$

where $\alpha = l, \rho, \lambda, r$. This solution can be obtained from Eq. (3) using the equalities

$$c_r = c^B, \quad c_\rho = c^A e^{-i\mathbf{k} \cdot \delta_1}, \quad c_\lambda = c^B e^{-i\mathbf{k} \cdot \mathbf{a}_1}, \quad c_l = c^A e^{-i2ak_x}. \quad (12)$$

The Brillouin zones corresponding to hexagonal and rectangular unit cells are shown in Fig. 1c. Compared to the area of the Brillouin zone of the hexagonal unit cell, the area of the Brillouin zone of the rectangular unit cell is two times smaller. Smaller Brillouin zone leads to the appearance of additional dispersion branches. Those dispersion branches can be taken into account by using two values of the wave vector κ in Eqs. (10) and (7), the one with $-\pi \leq \kappa < \pi$ and another obtained replacing κ by $2\pi + \kappa$. Using Eqs. (7), (12) we obtain the coefficients of the eigenvectors

$$c_r = 1, \quad c_\rho = -e^{-i\frac{\xi}{2}} \frac{\phi(\kappa, \xi)}{E(\kappa, \xi)}, \quad (13)$$

$$c_l = -s_3 e^{-i\frac{\kappa}{2}} \frac{\phi(\kappa, \xi)}{E(\kappa, \xi)}, \quad c_\lambda = s_3 e^{-i\frac{1}{2}(\kappa + \xi)}, \quad (14)$$

where

$$\phi(\kappa, \xi) = s_3 e^{-i\frac{\kappa}{2}} + 2 \cos\left(\frac{\xi}{2}\right) \quad (15)$$

and $s_3 = \pm 1$ indicates the dispersion branches that appear due to the smaller Brillouin zone. The equation for the energy now becomes

$$E(\kappa, \xi) = s_1 \sqrt{1 + 4 \cos^2\left(\frac{\xi}{2}\right) + s_3 4 \cos\left(\frac{\xi}{2}\right) \cos\left(\frac{\kappa}{2}\right)}. \quad (16)$$

This equation has been obtained in²³. Zero energy points of the graphene honeycomb lattice with dispersion relation (10) are at the points $K = (2\pi, 2\pi/3)$ and $K' = (2\pi, -2\pi/3)$, where coordinates are given in (κ, ξ) space. K points correspond to the corners of the first Brillouin zone. Using the Brillouin zone corresponding to the rectangular unit cell, the zero energy points have coordinates $(0, \pm \frac{2\pi}{3})$ and the number of these points is only two, as it is shown in Fig. 1c.

Since we will consider finite-size graphene sheets, evanescent solutions become important. Solution exponentially decreasing or increasing in the x -direction can be obtained by taking $\kappa = i|\kappa|$ in Eqs. (13), (14) and (16), whereas solution exponentially decreasing or increasing in the y -direction can be obtained by taking $\xi = i|\xi|$. The dependency of the energy on κ when $\xi = 0$ is shown in Fig. 2. We see that the branches with real and imaginary κ do not intersect at $|\kappa| > 0$.

B. Electron spectrum in various single layer graphene structures

From the boundary conditions we get restrictions on the possible values of the wave vectors κ , ξ . We will consider the structures of graphene that have a set of N rectangular unit cells in the x (armchair) direction and a set of $\mathcal{N} + 1/2$ rectangular unit cells in the y (zigzag) direction, so that there are \mathcal{N} hexagons along the y axis. Note that rectangular unit cell shown in Fig. 1b extends over the whole hexagon in the y direction, whereas it extends over more than one hexagon in x direction.

Using periodic boundary condition, corresponding to the graphene torus, we get that the possible values of the wave vectors κ , ξ are

$$\xi_j = \frac{2\pi}{\mathcal{N}} j, \quad j = -\left\lfloor \frac{\mathcal{N}}{2} \right\rfloor, -\left\lfloor \frac{\mathcal{N}}{2} \right\rfloor + 1, \dots, \left\lfloor \frac{\mathcal{N}-1}{2} \right\rfloor \quad (17)$$

$$\kappa_\nu = \frac{2\pi}{N} \nu, \quad \nu = -\left\lfloor \frac{N}{2} \right\rfloor, -\left\lfloor \frac{N}{2} \right\rfloor + 1, \dots, \left\lfloor \frac{N-1}{2} \right\rfloor \quad (18)$$

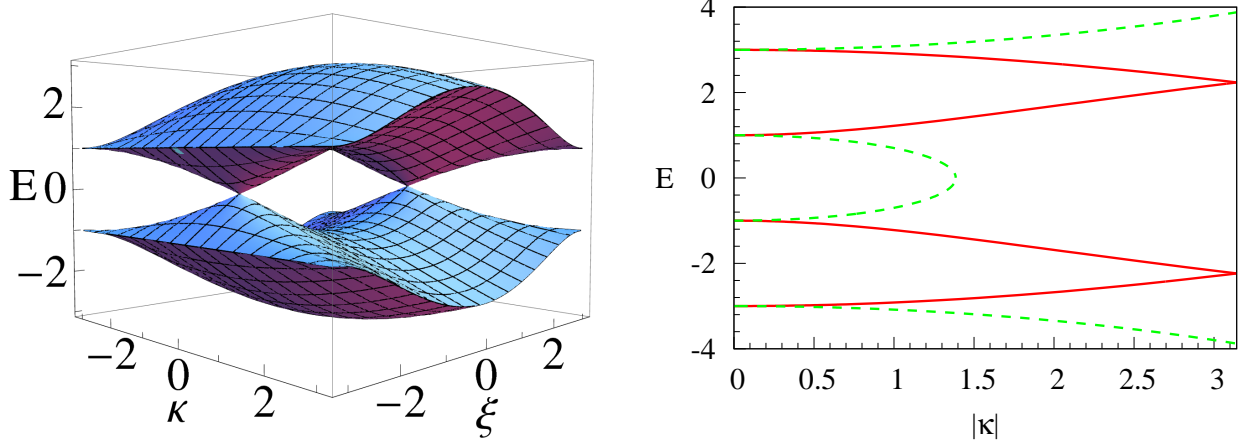


FIG. 2. (Color online) Left: dispersion branches of graphene for rectangular unit cell, calculated according to Eq. (16). Right: dispersion branches for $\xi = 0$, showing propagating solutions (red solid) and evanescent solutions (green dashed).

Here $[\cdot]$ denotes the integer part of a number. Thus the spectrum of graphene torus is given by Eq. (16) replacing κ and ξ by κ_ν and ξ_j .

For graphene armchair nanotubes one has the periodic boundary condition in the x direction and the requirement $\psi_{0,n,r} = \psi_{0,n,l} = \psi_{\mathcal{N}+1,n,l} = \psi_{\mathcal{N}+1,n,r} = 0$ for the y direction. Since the energy (16), does not depend on the sign of wave vector ξ , we will search for the eigenvectors of the Hamiltonian (1) as a superposition of periodic solutions Eq. (11) with ξ and $-\xi$,

$$\psi_{m,n,\alpha} = ac_\alpha(\xi, \kappa_\nu)e^{i\xi m + i\kappa_\nu n} + bc_\alpha(-\xi, \kappa_\nu)e^{-i\xi m + i\kappa_\nu n}, \quad (19)$$

where κ_ν is given by Eq. (18) and ξ needs to be determined. From the boundary conditions we get a system of two equations for the coefficients a and b

$$ac_{r,l}(\xi, \kappa_\nu) + bc_{r,l}(-\xi, \kappa_\nu) = 0, \quad (20)$$

$$ae^{i\xi(\mathcal{N}+1)}c_{r,l}(\xi, \kappa_\nu) + be^{-i\xi(\mathcal{N}+1)}c_{r,l}(-\xi, \kappa_\nu) = 0. \quad (21)$$

This system of equations has non-zero solutions only when the determinant is zero. From Eqs. (13), (14) it follows that the coefficients $c_{r,l}(\xi, \kappa)$ do not depend on the sign of ξ and we get the condition $\sin(\xi(\mathcal{N}+1)) = 0$ or

$$\xi = \frac{\pi j}{\mathcal{N}+1}, \quad j = 1, \dots, \mathcal{N} \quad (22)$$

Additionally, there are two N -fold degenerate levels corresponding to $\xi = \pi$ with energies $E = \pm 1$. The states of those levels have zero wave function amplitudes at the l and r sites.

For graphene zigzag nanotubes one has the periodic boundary condition in the y direction and the condition $\psi_{m,0,r} = \psi_{m,N+1,l} = 0$ for the x direction. Similarly as for the armchair nanotubes, the energy (16), does not depend on the sign of wave vector κ , and we search for the eigenvectors of the Hamiltonian (1) as a superposition of periodic solutions Eq. (11) with κ and $-\kappa$,

$$\psi_{m,n,\alpha} = ac_\alpha(\xi_j, \kappa)e^{i\xi_j m + i\kappa n} + bc_\alpha(\xi_j, -\kappa)e^{i\xi_j m - i\kappa n}, \quad (23)$$

where ξ_j is given by Eq. (17) and κ needs to be determined. From the boundary conditions we get a system of two equations for the coefficients a and b

$$ac_r(\xi_j, \kappa) + bc_r(\xi_j, -\kappa) = 0, \quad (24)$$

$$ae^{i\kappa(N+1)}c_l(\xi_j, \kappa) + be^{-i\kappa(N+1)}c_l(\xi_j, -\kappa) = 0. \quad (25)$$

Using Eqs. (13), (14) we obtain that non-zero solutions are possible when

$$\frac{\sin(\kappa N)}{\sin(\kappa(N + \frac{1}{2}))} = -s_3 2 \cos\left(\frac{\xi_j}{2}\right). \quad (26)$$

The possible values of wave vector κ should obey this equation. The same condition has been obtained in Ref. 23. Equation (26) allows for the imaginary values of wave vector κ . The imaginary values appear when $\xi^c < |\xi_j| < \pi$ and $s_3 = -1$, where the critical value $\xi^c = 2 \arccos(N/(2N+1))$ of the wave vector ξ is obtained from Eq. (26) setting $\kappa = 0$. In the limit $N \rightarrow \infty$ from the condition (26) with imaginary κ and Eq. (16) follows that $E = 0$: edge states near zigzag edges in the semi-infinite system have zero energy.

For $N \times \mathcal{N}$ sheet of graphene open boundary conditions in the y direction are the same as for armchair nanotubes and in the x direction are the same as for zigzag nanotubes. Since the resulting conditions for the wave vectors κ , ξ are not coupled, the eigenvector of the Hamiltonian (1) is a superposition of four periodic solutions having all possible combinations of the signs of κ and ξ and the possible values of the wave vectors are given by Eqs. (22) and (26). In addition there are two N -fold degenerate levels corresponding to $\xi = \pi$ with energies $E = \pm 1$.

III. BILAYER GRAPHENE

Now we will consider the spectrum of π electrons in bilayer graphene. The tight-binding Hamiltonian for electrons in bilayer graphene has the form

$$H_{\text{bi}} = V \sum_j (a_{j,2}^\dagger a_{j,2} + b_{j,2}^\dagger b_{j,2} - a_{j,1}^\dagger a_{j,1} - b_{j,1}^\dagger b_{j,1}) - t \sum_{\langle i,j \rangle, p} (a_{i,p}^\dagger b_{j,p} + b_{j,p}^\dagger a_{i,p}) - t_\perp \sum_j (a_{j,1}^\dagger a_{j,2} + a_{j,2}^\dagger a_{j,1}), \quad (27)$$

where the operators $a_{i,p}$ and $b_{i,p}$ annihilate an electron on sublattice A_p at site $\mathbf{R}_i^{A_p}$ and on sublattice B_p at site $\mathbf{R}_i^{B_p}$, respectively. The index $p = 1, 2$ numbers the layers in the bilayer system. In the Hamiltonian (27) we neglected the terms corresponding to the hopping between atom B_1 and atom B_2 , with the hopping energy γ_3 , and the terms corresponding to the hopping between atom A_1 (A_2) and atom B_2 (B_1) with the hopping energy γ_4 . Neglect of those hopping terms leads to the minimal model of bilayer graphene²⁸. The parameter t_\perp ($t_\perp \approx 0.4 \text{ eV}$) is the hopping energy between atom A_1 and atom A_2 while V is half the shift in the electrochemical potential between the two layers. Similarly as for the monolayer graphene, we will express all the energies in the units of t .

A. Electron spectrum in infinite sheet of bilayer graphene

We will proceed similarly as in the previous Section and will analyze an infinite system at first. The atoms in the sublattices A_1 and A_2 are positioned at $\mathbf{R}_{p,q}^{A_{1,2}} = p\mathbf{a}_1 + q\mathbf{a}_2$, in the sublattice B_1 the atoms are positioned at $\mathbf{R}_{p,q}^{B_1} = \boldsymbol{\delta}_1 + p\mathbf{a}_1 + q\mathbf{a}_2$ and in the sublattice B_2 the atoms are positioned at $\mathbf{R}_{p,q}^{B_2} = -\boldsymbol{\delta}_1 + p\mathbf{a}_1 + q\mathbf{a}_2$. We search for the eigenvectors of the Hamiltonian (27) in the form of the plane waves. The probability amplitudes to find an atom in the sites $\mathbf{R}_{p,q}^{A_{1,2}}$ and $\mathbf{R}_{p,q}^{B_{1,2}}$ of the sublattices A_j and B_j are

$$\psi_{p,q}^{A_{1,2}} = c^{A_{1,2}} e^{i\mathbf{k} \cdot \mathbf{R}_{p,q}^{A_{1,2}}}, \quad \psi_{p,q}^{B_{1,2}} = c^{B_{1,2}} e^{i\mathbf{k} \cdot \mathbf{R}_{p,q}^{B_{1,2}}}. \quad (28)$$

The coefficients c^{A_p} and c^{B_p} obey the eigenvalue equations

$$-Ec^{A_1} = Vc^{A_1} + c^{B_1} \tilde{\phi}(\mathbf{k}) + \gamma c^{A_2}, \quad (29)$$

$$-Ec^{B_1} = Vc^{B_1} + c^{A_1} \tilde{\phi}(-\mathbf{k}), \quad (30)$$

$$-Ec^{A_2} = -Vc^{A_2} + c^{B_2} \tilde{\phi}(-\mathbf{k}) + \gamma c^{A_1}, \quad (31)$$

$$-Ec^{B_2} = -Vc^{B_2} + c^{A_2} \tilde{\phi}(\mathbf{k}). \quad (32)$$

Here energy E , potential V and interaction between layers $\gamma \equiv t_\perp/t$ are in the units of the hopping integral t . Using the nearest-neighbor hopping energy $t \approx 2.8 \text{ eV}$ and the hopping energy between two layers $t_\perp \approx 0.4 \text{ eV}$ one gets $\gamma \approx 0.14$. When $V = 0$, the π electron spectrum is determined by the equation

$$E(\mathbf{k}) = s_1 \left(s_2 \frac{\gamma}{2} + \sqrt{\frac{\gamma^2}{4} + |\tilde{\phi}(\mathbf{k})|^2} \right), \quad (33)$$

where $s_1, s_2 = \pm 1$. The coefficients of the eigenvector are

$$\begin{aligned} c^{A_1} &= -\frac{E(\mathbf{k})}{\tilde{\phi}(-\mathbf{k})}, & c^{B_1} &= 1, \\ c^{A_2} &= s_1 s_2 \frac{E(\mathbf{k})}{\tilde{\phi}(-\mathbf{k})}, & c^{B_2} &= -s_1 s_2 \frac{\tilde{\phi}(\mathbf{k})}{\tilde{\phi}(-\mathbf{k})}. \end{aligned} \quad (34)$$

When $V \neq 0$ the spectrum is

$$E(\mathbf{k}) = s_1 \sqrt{\frac{\gamma^2}{2} + V^2 + |\tilde{\phi}(\mathbf{k})|^2} + s_2 \sqrt{\frac{\gamma^4}{4} + |\tilde{\phi}(\mathbf{k})|^2 (4V^2 + \gamma^2)} \quad (35)$$

and the coefficients of the eigenvector are

$$\begin{aligned} c^{A_1} &= -\frac{E(\mathbf{k}) + V}{\tilde{\phi}(-\mathbf{k})}, & c^{B_1} &= 1, \\ c^{A_2} &= \frac{E(\mathbf{k}) - V}{\tilde{\phi}(-\mathbf{k})} f(\mathbf{k}), & c^{B_2} &= -\frac{\tilde{\phi}(\mathbf{k})}{\tilde{\phi}(-\mathbf{k})} f(\mathbf{k}), \end{aligned} \quad (36)$$

where the function

$$f(\mathbf{k}) = \frac{(E(\mathbf{k}) + V)^2 - |\tilde{\phi}(\mathbf{k})|^2}{\gamma(E(\mathbf{k}) - V)} \quad (37)$$

describes the contribution of the second sheet of graphene to the eigenvector.

Finite-size bilayer graphene sheets can be in AB- α or AB- β stacking, as is shown in Fig. 3a,b. Similarly as for graphene monolayer, we will use rectangular unit cells, one shifted with respect to the other, in each layer of bilayer graphene. However, the position of rectangular cells are different for different stacking types. Rectangular unit cells have eight atoms with labels $l_1, \lambda_1, \rho_1, r_1$ and $l_2, \lambda_2, \rho_2, r_2$, as is shown in Fig. 3c,d. For the AB- α stacking the atoms with labels l_1, ρ_1 belong to the sublattice A_1 , atoms λ_1, r_1 to the sublattice B_1 , atoms l_2, ρ_2 to the sublattice A_2 and atoms λ_2, r_2 to the sublattice B_2 . For the AB- β stacking the atoms with labels l_1, ρ_1 belong to the sublattice B_1 , atoms λ_1, r_1 to the sublattice A_1 , atoms l_2, ρ_2 to the sublattice B_2 and atoms λ_2, r_2 to the sublattice A_2 .

We search for the solutions of the form

$$\psi_{m,n,\alpha_p} = c_{\alpha_p} e^{i\xi m + i\kappa n} \quad (38)$$

where $\alpha = l, \rho, \lambda, r$ is the label of atoms and $p = 1, 2$ is the number of the layer. For the AB- α stacking this solution can be obtained from Eq. (28) using the equalities

$$c_{r_1} = c^{B_1}, \quad c_{\rho_1} = c^{A_1} e^{-i\mathbf{k} \cdot \boldsymbol{\delta}_1}, \quad c_{\lambda_1} = c^{B_1} e^{-i\mathbf{k} \cdot \mathbf{a}_1}, \quad c_{l_1} = c^{A_1} e^{-i2ak_x}, \quad (39)$$

$$c_{r_2} = c^{B_2} e^{-iak_x}, \quad c_{\rho_2} = c^{A_2} e^{-i\mathbf{k} \cdot \boldsymbol{\delta}_1}, \quad c_{\lambda_2} = c^{B_2} e^{i\mathbf{k} \cdot \boldsymbol{\delta}_2}, \quad c_{l_2} = c^{A_2} e^{iak_x} \quad (40)$$

whereas for the AB- β stacking the coefficients are

$$c_{r_1} = (c^{A_1})^*, \quad c_{\rho_1} = (c^{B_1})^* e^{-i\mathbf{k} \cdot \boldsymbol{\delta}_1}, \quad c_{\lambda_1} = (c^{A_1})^* e^{-i\mathbf{k} \cdot \mathbf{a}_1}, \quad c_{l_1} = (c^{B_1})^* e^{-i2ak_x}, \quad (41)$$

$$c_{r_2} = (c^{A_2})^* e^{-i\mathbf{k} \cdot \mathbf{a}_2}, \quad c_{\rho_2} = (c^{B_2})^* e^{-iak_x}, \quad c_{\lambda_2} = (c^{A_2})^*, \quad c_{l_2} = (c^{B_2})^* e^{i\mathbf{k} \cdot \boldsymbol{\delta}_1}. \quad (42)$$

Similarly as for monolayer graphene, to take into account the smaller Brillouin zone we need two dispersion branches: one with κ and one with $2\pi + \kappa$. Using Eq. (34) or Eq. (36) we obtain the coefficients of the eigenvectors. The expressions for the coefficients are presented in Appendix A. The expression for the energy becomes

$$E(\kappa, \xi) = s_1 \sqrt{\frac{\gamma^2}{2} + V^2 + |\phi(\kappa, \xi)|^2} + s_2 \sqrt{\frac{\gamma^4}{4} + |\phi(\kappa, \xi)|^2 (4V^2 + \gamma^2)} \quad (43)$$

which reduces to

$$E(\kappa, \xi) = s_1 \left(s_2 \frac{\gamma}{2} + \sqrt{\frac{\gamma^2}{4} + |\phi(\kappa, \xi)|^2} \right) \quad (44)$$

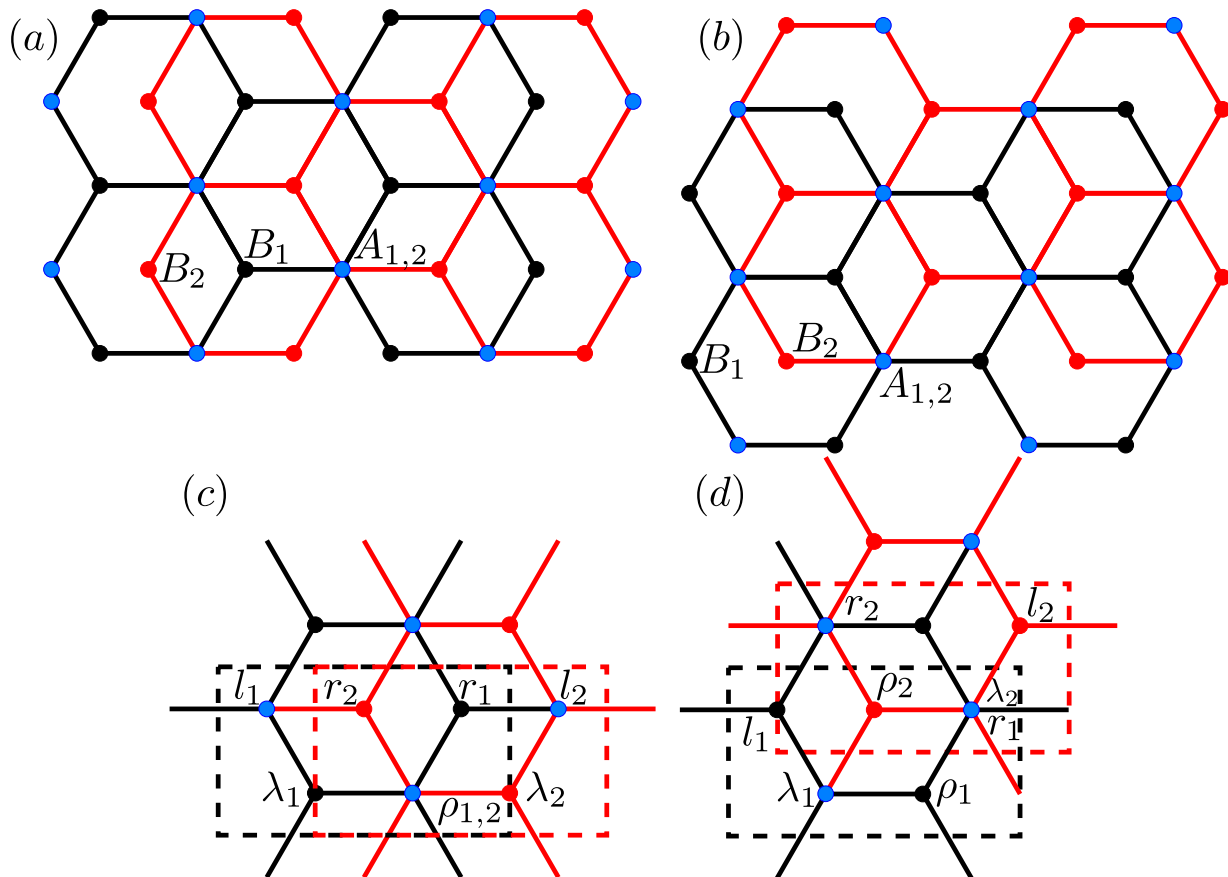


FIG. 3. (Color online) Upper part: sublattices A_1 , A_2 , B_1 , B_2 on bilayer graphene in AB- α stacking (a) and AB- β stacking (b). Lower part: indication of labels of carbon atoms used in the description of the π electron spectrum for the bilayer graphene with AB- α stacking (c) and AB- β stacking (d).

for $V = 0$. Here

$$|\phi(\kappa, \xi)|^2 = 1 + 4 \cos^2 \left(\frac{\xi}{2} \right) + s_3 4 \cos \left(\frac{\xi}{2} \right) \cos \left(\frac{\kappa}{2} \right) \quad (45)$$

and $s_3 = \pm 1$ indicates the dispersion branches that appear due to the smaller Brillouin zone.

In addition to the propagating waves, for finite-size bilayer graphene sheets evanescent solutions become important. Solution exponentially decreasing or increasing in the x -direction can be obtained by taking $\kappa = i|\kappa|$. Solution exponentially decreasing or increasing in the y -direction can be obtained by taking $\xi = i|\xi|$. In addition to the purely imaginary ξ there are solutions, corresponding to $s_3 = -1$, having complex values of ξ . The dependency of the energy on the wave vector κ when the wave vector ξ is constant and on the wave vector ξ when the wave vector κ is constant is shown in Fig. 4. We see that now, in contrast to the graphene monolayer, the branches with real and imaginary κ can have the same energy.

B. Electron spectrum in various bilayer graphene structures

We will consider the structures of bilayer graphene that have a set of N rectangular unit cells in the x (armchair) direction and a set of $\mathcal{N} + 1/2$ rectangular unit cells in the y (zigzag) direction, so that there are \mathcal{N} hexagons along the y axis. Note that the rectangular unit cells shown in Figs. 3c and 3d extend over the whole hexagon in the y direction, whereas they extend over more than one hexagon in x direction. In principle, in the case of bilayer graphene nanotubes the numbers N or \mathcal{N} in for the inner and outer cylinders are different. However, for simplicity we will consider them as the same, which is a good approximation for sufficiently large tubes when $N \rightarrow \infty$ or $\mathcal{N} \rightarrow \infty$.

Similarly as for graphene monolayer, from the boundary conditions we get restrictions on the possible values of the wave vectors κ , ξ . Using periodic boundary condition, corresponding to the bilayer graphene torus, we get that the

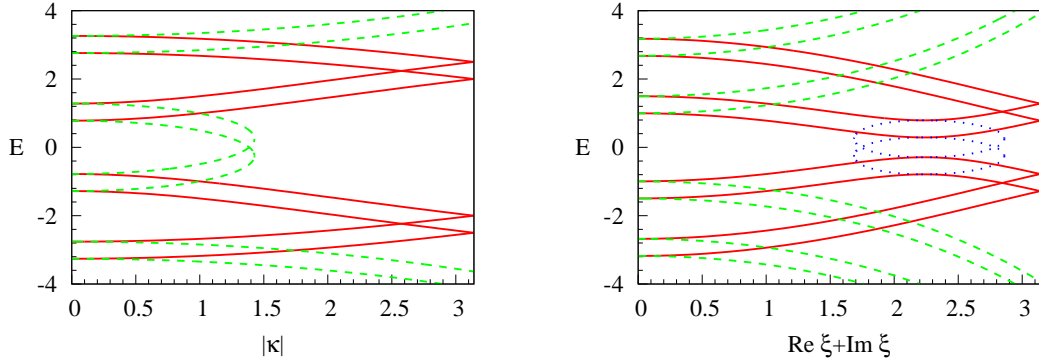


FIG. 4. (Color online) Dispersion branches of bilayer graphene: dependency of the energy on the wave vector κ when the wave vector ξ is constant ($\xi = 0$) (left) and on the wave vector ξ when the wave vector κ is constant ($\kappa = 1.0$) (right). Propagating solutions are shown with red solid line, evanescent solutions with green dashed line, and evanescent oscillating solutions with complex value of the wave vector ξ are shown with blue dotted line. In order to show the structure of the dispersion branches more clearly, the value of the parameter γ is set sufficiently large, $\gamma = 0.5$.

possible values of the wave vectors κ , ξ are given by Eqs. (17), (18).

For bilayer graphene armchair nanotubes one has the periodic boundary condition in the x direction and the condition

$$\psi_{0,n,r_p} = \psi_{0,n,l_p} = \psi_{N+1,n,l_p} = \psi_{N+1,n,r_p} = 0 \quad (46)$$

for the y direction. Here $p = 1, 2$ is the number of the layer. This condition is the same for both the AB- α and AB- β stackings. For bilayer graphene with AB- α stacking the coefficients $c_{r_p,l_p}(\xi, \kappa)$ do not depend on the sign of ξ and we get the same conditions (18), (22) for the wave vectors κ , ξ , as for the monolayer graphene armchair tubes.

For bilayer graphene with AB- β stacking the coefficients $c_{r_p,l_p}(\xi, \kappa)$ depend on the sign of ξ , and condition for the possible values of the wave vector ξ is much more complicated. There are eight boundary conditions in the y direction. In bilayer graphene there are four eigenstates with different wave vectors along y direction, $\xi^{(1)}$, $\xi^{(2)}$, $\xi^{(3)}$ and $\xi^{(4)}$, having the same energy: $E(\kappa, \xi^{(1)}) = E(\kappa, \xi^{(2)}) = E(\kappa, \xi^{(3)}) = E(\kappa, \xi^{(4)})$, as is evident from Fig. 4. Two or four of the wave vectors $\xi^{(1)}$, $\xi^{(2)}$, $\xi^{(3)}$, $\xi^{(4)}$ can be imaginary or complex numbers. Since the energy does not depend on the sign of ξ , we can form a wave function from superposition of eight waves. From the boundary conditions (46) resulting resulting set of linear equations can have nonzero solution only if 8×8 determinant is zero. Analytical form of this condition in is too large and too complicated to be useful.

For bilayer graphene zigzag nanotubes one has the periodic boundary condition in the y direction and the condition

$$\psi_{m,0,r_1} = \psi_{m,N+1,l_1} = \psi_{m,0,l_2} = \psi_{m,N+1,r_2} = 0 \quad (47)$$

for the x direction. Here $p = 1, 2$ is the number of the layer. This condition is the same for both the AB- α and AB- β stackings. In the bilayer graphene there are two eigenstates with wave vectors along x direction, $\kappa^{(1)}$ and $\kappa^{(2)}$, having different absolute values but corresponding the same energy: $E(\kappa^{(1)}, \xi) = E(\kappa^{(2)}, \xi)$. One or both of the wave vectors $\kappa^{(1)}$, $\kappa^{(2)}$ can be imaginary. The energy can be equal only if the signs s_1 , s_2 obey the condition

$$s_1^{(2)} s_2^{(2)} = -s_1^{(1)} s_2^{(1)} \quad (48)$$

When the bias potential is zero, $V = 0$, from the equality of the energy we can express $\kappa^{(2)}$:

$$s_3^{(2)} \cos\left(\frac{\kappa^{(2)}}{2}\right) = s_3^{(1)} \cos\left(\frac{\kappa^{(1)}}{2}\right) + s_1^{(1)} s_2^{(1)} \frac{\gamma}{2 \cos\left(\frac{\xi}{2}\right)} E(\kappa^{(1)}, \xi) \quad (49)$$

When $V \neq 0$ then

$$s_3^{(2)} \cos\left(\frac{\kappa^{(2)}}{2}\right) = s_3^{(1)} \cos\left(\frac{\kappa^{(1)}}{2}\right) \pm \frac{\gamma}{2 \cos\left(\frac{\xi}{2}\right)} \sqrt{4E^2V^2 + \gamma^2(E^2 - V^2)} \quad (50)$$

There are four boundary conditions in the x direction. Since the energy does not depend on the sign of κ , we can form a wave function from superposition of four waves. From the boundary conditions (47) resulting set of linear

equations can have nonzero solution only if 4×4 determinant is zero. The possible values of the wave vector ξ is given by Eq. (17), and the conditions for the possible values of the wave vector κ are given in the Appendix B.

For $N \times \mathcal{N}$ sheet of bilayer graphene open boundary conditions in the y direction are the same as for armchair nanotubes, Eq. (46) and in the x direction are the same as for zigzag nanotubes, Eq. (47). For AB- α stacking, the conditions for the possible values of the wave vectors κ, ξ are combination of the conditions for zigzag and armchair bilayer graphene tubes. Specifically, when $V = 0$, the conditions are given by Eqs. (22) and (B1) or (B2). When $V \neq 0$ then the conditions are given by Eqs. (22) and (B3). For AB- β stacking it is impossible to separate conditions for the wave vector ξ from the conditions for the wave vector κ . The resulting expressions are very large and complicated.

C. Summary of the possible values of wave vectors

For structures of bilayer graphene, the energy spectrum is completely determined by Eq. (44) or (43) with appropriate expressions for wave vectors κ and ξ .

Equations presented in Appendix B make one quantum number dependent on the other. This dependence appears because of zigzag-shaped edges. For structures where zigzag edges do not exist or their effect can be disregarded the wave vector κ_ν can be replaced by a continuous variable.

Thus, the possible values of wave vectors for various structures are as follows:

- For the armchair bilayer graphene ribbon of infinite length with AB- α stacking, the wave vectors are determined by

$$0 \leq \kappa \leq \pi, \quad \xi_j = \frac{\pi j}{\mathcal{N} + 1}, \quad j = 1, \dots, \mathcal{N} \quad (51)$$

- For the armchair bilayer graphene ribbon of infinite length with AB- β staking we have $0 \leq \kappa \leq \pi$ and the equation for the possible values of ξ is complicated.
- For the zigzag bilayer graphene ribbon of infinite length we have $0 \leq \xi \leq \pi$, the conditions for the possible values of κ , given in Appendix B, are different for AB- α and AB- β stackings.
- For the zigzag bilayer carbon tube of infinite length with AB- α or AB- β stacking, the wave vectors are determined by

$$0 \leq \kappa \leq \pi, \quad \xi_j = \frac{2\pi}{\mathcal{N}} j, \quad j = -\left\lfloor \frac{\mathcal{N}}{2} \right\rfloor, -\left\lfloor \frac{\mathcal{N}}{2} \right\rfloor + 1, \dots, \left\lfloor \frac{\mathcal{N} - 1}{2} \right\rfloor \quad (52)$$

- For the armchair bilayer carbon tube of infinite length with AB- α or AB- β stacking:

$$\kappa_\nu = \frac{2\pi}{N} \nu, \quad \nu = -\left\lfloor \frac{N}{2} \right\rfloor, -\left\lfloor \frac{N}{2} \right\rfloor + 1, \dots, \left\lfloor \frac{N - 1}{2} \right\rfloor, \quad 0 \leq \xi \leq \pi. \quad (53)$$

Taking into account the ranges of the possible values of the wave vectors, zero energy points for various structures with bias potential $V = 0$ are as follows:

- For zigzag bilayer carbon tube zero energy points are $(0, \frac{2\pi}{3})$, $(0, -\frac{2\pi}{3})$.
- For armchair bilayer carbon tube, zero energy point is $(0, \frac{2\pi}{3})$.
- The dispersion of armchair bilayer graphene ribbon has only one zero-energy point $(0, \frac{2\pi}{3})$
- For zigzag bilayer graphene ribbon dispersion this point cannot be shown in the real plane.

IV. BAND STRUCTURE NEAR THE FERMI ENERGY

In this Section only a part of the spectrum with smallest absolute value of the energy is in focus. This part corresponds to $s_2 = -1$, $s_3 = -1$. In order to obtain an approximate expression for the energy spectrum near the

Fermi energy we expand Eq. (45) in power series near the zero point $\kappa = 0$, $\xi = 2\pi/3$, yielding

$$\begin{aligned} |\phi(\kappa, \xi)|^2 &\approx \frac{3}{4} \left[\frac{\kappa^2}{3} \left(1 - \frac{\sqrt{3}}{2}q \right) + q^2 \left(1 + \frac{q}{2\sqrt{3}} \right) \right] \\ &\approx \frac{3}{4} \left(\frac{\kappa^2}{3} + \left(q - \frac{\kappa^2}{4\sqrt{3}} \right)^2 \right). \end{aligned} \quad (54)$$

Here $q \equiv \xi - 2\pi/3$ and $|\kappa| \ll 1$, $|q| \ll 1$. Substituting Eq. (54) into Eq. (44) or Eq. (43) one obtains the approximate expression for the energy spectrum. Thus, when the bias potential is zero $V = 0$, the approximate expression for the energy is

$$E(\kappa, \xi) = s_1 \left(-\frac{\gamma}{2} + \sqrt{\frac{\gamma^2}{4} + \frac{3}{4} \left(\frac{\kappa^2}{3} + \left(q - \frac{\kappa^2}{4\sqrt{3}} \right)^2 \right)} \right) \quad (55)$$

Furthermore, assuming that $|\phi(\kappa, \xi)|^2 \ll \gamma$, the branch of Eq. (44) with $s_2 = -1$, $s_3 = -1$ takes the form

$$E(\kappa, \xi) \approx s_1 \frac{|\phi(\kappa, \xi)|^2}{\gamma} \quad (56)$$

When $V \neq 0$ and $V \ll \gamma$, then Eq. (43) becomes

$$E(\kappa, \xi) \approx s_1 V - s_1 \frac{2V}{\gamma^2} |\phi(\kappa, \xi)|^2 + s_1 \frac{|\phi(\kappa, \xi)|^4}{2V\gamma^2} \quad (57)$$

The bilayer graphene has a gap at $|\phi(\kappa, \xi)|^2 = 2V^2$. However, since the parameter γ is small, $\gamma \ll 1$, the approximate expressions (56), (57) are suitable only for very small values of $|\kappa|$ and $|q|$.

The spectrum of various structures of bilayer graphene can be obtained from the approximate expressions for $|\phi(\kappa, \xi)|^2$ near zero points. In contrast to Eqs. (56) and (57), the energy of monolayer graphene is $E(\kappa, \xi) = s_1 \sqrt{|\phi(\kappa, \xi)|^2}$. Thus, the analysis of the square root of $|\phi(\kappa, \xi)|^2$ essentially was done in Ref. 23. Going back to the original wave vectors k_x and k_y , the band structure of bilayer graphene tubes and ribbons when $V = 0$ similarly as in Ref. 23 can be summarized by the equation

$$E_\nu(k_\parallel) \approx s_1 \left(-\frac{\gamma}{2} + \sqrt{\frac{\gamma^2}{4} + \frac{9}{4} a^2 [(k_\parallel - \bar{k}_\parallel)^\sigma]^2 + k_{\perp\nu}^{\sigma 2}} \right), \quad (58)$$

where k_\parallel and $k_{\perp\nu}$ denote the longitudinal (continuous) and the transverse (quantized) components of the wave vector, respectively. Index σ specifies the structure. Further in this Section we will consider only the case when $V = 0$.

A. Quantum conductance

Within the framework of the Landauer approach³³⁻³⁵, the zero-temperature conductance of a ideal wire is equal to

$$G(E) = \frac{2e^2}{h} \sum_\nu g_\nu T_\nu(E) \quad (59)$$

where $2e^2/h$ is conductance quantum, g_ν is the band degeneracy, and transmission coefficient T_ν is zero or unity depending on whether the ν -th band is open or closed for charge carriers with energy E .

When bias potential is zero, $V = 0$, the transmission coefficient is $T_\nu(E) = \Theta(E - E_\nu^\sigma)$ for conduction bands and $T_\nu(E) = \Theta(|E - E_\nu^\sigma|)$ for valence bands. Here E_ν^σ are the subband threshold energies and $\Theta(x)$ is the Heaviside step function. When the approximation Eq. (58) is valid, the subband threshold energies are

$$E_\nu^\sigma = s_1 \left(-\frac{\gamma}{2} + \sqrt{\frac{\gamma^2}{4} + \frac{9}{4} a^2 k_{\perp\nu}^{\sigma 2}} \right). \quad (60)$$

The degeneracies are shown in Table I. The values of g_ν for armchair bilayer carbon tube and zigzag bilayer graphene ribbon with $\nu > 1$, represented in Table I should be doubled, because electron or hole states with $\pm k_\parallel \neq 0$ are degenerate.

TABLE I. Degeneracy g_ν^σ of the ν -th band energy $|E_\nu^\sigma(k_\parallel = 0)|$

σ	g_ν^σ
armchair bilayer carbon tube	$1(\nu = 0), 2(\nu \neq 0)$
zigzag bilayer carbon tube	2
armchair bilayer graphene ribbon	1
zigzag bilayer graphene ribbon	1

The electron or hole conductance of armchair and zigzag bilayer carbon tubes and their parent graphene ribbons has thus the form of a ladder, symmetrically ascending with the increase in energy for electrons, and with the decrease of energy for holes. For the charge carrier energy that falls between the n -th and $(n+1)$ -th bands, the wire conductance equals

$$G(E) = \frac{2e^2}{h} \begin{cases} n & \text{armchair bilayer ribbon} \\ 2n+2 & \text{zigzag bilayer ribbon} \\ 2n & \text{zigzag bilayer carbon tube} \\ 2(2n+1) & \text{armchair bilayer carbon tube} \end{cases} \quad (61)$$

The conductance for bilayer graphene ribbons has been numerically calculated in Ref. 30. The expression (61) for the conductance coincides with that of Ref. 30.

B. Density of states

The density of states (DOS) of a quantum wire, including a factor 2 for the spin degeneracy, reads

$$\rho(E) = \frac{2}{\pi} \sum_\nu \left(\frac{dE_\nu(k_\parallel, k_{\perp\nu})}{dk_\parallel} \right)^{-1}. \quad (62)$$

The summation includes all transverse modes with energy $E_\nu \leq E$. Using Eq. (58) we obtain the DOS of bilayer graphene

$$\rho(E) = \frac{2}{3\pi a} \sum_\nu g_\nu \frac{(2|E| + \gamma)}{\sqrt{(|E| - |E_\nu^\sigma|)(|E| + |E_\nu^\sigma| + \gamma)}} \Theta(|E| - |E_\nu^\sigma|), \quad (63)$$

The index ν is $\nu = 0, \pm 1, \pm 2, \dots$ for bilayer graphene tubes and armchair bilayer graphene ribbons and $\nu = 0, 1, 2, \dots$ for the zigzag bilayer graphene ribbons. The electron density at zero temperature is obtained by the integration of the DOS from the charge neutrality point $\mu_0 = 0$ to the Fermi energy,

$$n = \int_0^{E_F} \rho(E) dE \quad (64)$$

Using Eq. (63) we get

$$n^\sigma(E_F) = \frac{4}{3\pi a} \sum_\nu g_\nu \sqrt{(|E_F| - |E_\nu^\sigma|)(|E_F| + |E_\nu^\sigma| + \gamma)} \Theta(|E_F| - |E_\nu^\sigma|) \quad (65)$$

C. Armchair bilayer carbon tube

For the armchair bilayer carbon tube we have that κ in Eq. (54) has discrete values $\kappa_\nu = 2\pi\nu/N$, $\nu = 0, \pm 1, \dots$ and q is continuous. Thus the energy spectrum has the form

$$E_\nu(k_y) = s_1 \left(-\frac{\gamma}{2} + \sqrt{\frac{\gamma^2}{4} + \frac{9}{4}a^2 \left[(k_y - \bar{k}_{y,\nu})^2 + \frac{4\pi^2\nu^2}{9a^2N^2} \right]} \right) \quad (66)$$

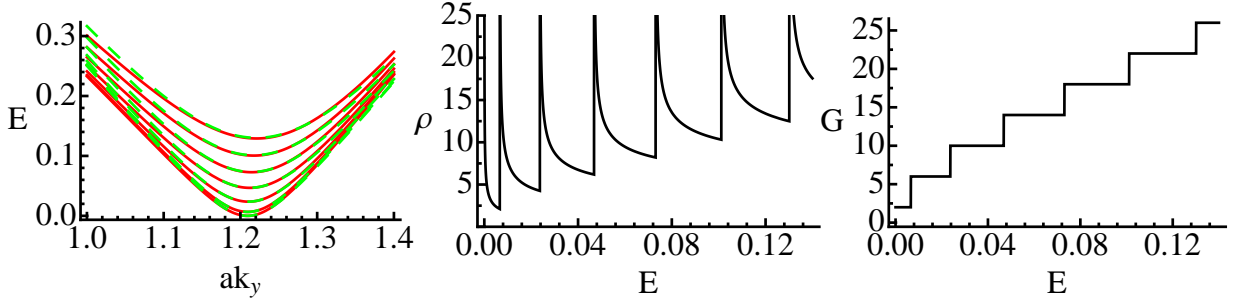


FIG. 5. (Color online) Band structure of armchair bilayer carbon tubes (left), DOS (center) and conductance (right). The number of rectangular unit cells in the x direction $N = 100$. Solid red lines are calculated according Eqs. (44), (45); dashed green lines represent approximation (66). Bands with $s_2 = +1$ are not shown. DOS is given in units of a^{-1} and is calculated according to Eqs. (63), (68). The conductance is given in units of $2e^2/h$ and is calculated using Eq. (61).

with

$$\bar{k}_{y,\nu} = \frac{2\pi}{3\sqrt{3}a} + \frac{\pi^2\nu^2}{3aN^2} \quad (67)$$

Conduction (valence) band bottoms (tops) are equal to

$$E_\nu = s_1 \left(-\frac{\gamma}{2} + \sqrt{\frac{\gamma^2}{4} + \frac{\pi^2\nu^2}{N^2}} \right) \quad (68)$$

The distance between the minima of the dispersion branches with the indices $s_2 = -1$ and $s_2 = +1$ is γ . The number ν of subbands with the index $s_2 = -1$ and energy smaller than the energies of the subbands with index $s_2 = +1$ is greater than 1 only when the number of rectangular unit cells in the x direction N is sufficiently large. Using the equation $E_{\nu,\max} = \gamma$ and estimating the subband threshold energy (68) as $E_\nu \approx \pi^2\nu^2/(\gamma N^2)$ one obtains that the requirement $\nu \gg 1$ leads to $N \gg \pi/\gamma$. In calculations we used $N = 100$.

The band structure, calculated with the use of exact Eqs. (44), (45) and approximated according to Eq. (66), is represented in Fig. 5. One sees that Eq. (66) provides accurate reproduction of exact results. Also is shown the DOS, calculated with Eqs. (63), (68), and the conductance $G(E) = (2e^2/h)2(2n + 1)$.

D. Zigzag bilayer carbon tube

Distinct from armchair bilayer carbon tubes, which are always metallic when $V = 0$, zigzag bilayer carbon tube has a gapless spectrum if $j^* \equiv \mathcal{N}/3$ is an integer, $E_{j=j^*}(\kappa = 0) = 0$. Otherwise, zigzag bilayer carbon tube spectrum has a gap. If $\mathcal{N}/3$ is not an integer, band index of the lowest conduction (highest valence) band can be equal either to $j^* \equiv (\mathcal{N}-1)/3$ or to $j^* \equiv (\mathcal{N}+1)/3$. As a result of expansion near zero-energy points in powers of κ and $2\pi(j-j^*)/\mathcal{N}$, we arrive at

$$|\phi(\kappa, \xi)|^2 \approx \frac{3}{4} \left(q_\nu^2 + \frac{\kappa^2}{3} \right) \quad (69)$$

where

$$q_\nu = \begin{cases} \frac{2\pi}{\mathcal{N}} |\nu - \frac{1}{3}| \ll 1, & \text{semiconducting} \\ \frac{2\pi|\nu|}{\mathcal{N}} \left(1 + \frac{\pi\nu}{2\sqrt{3}\mathcal{N}} \right) \ll 1, & \text{metallic} \end{cases}$$

with $\nu = 0, \pm 1, \dots$. The wave vector component κ is continuous. The energy spectrum has the form

$$E_\nu(k_x) = s_1 \left(-\frac{\gamma}{2} + \sqrt{\frac{\gamma^2}{4} + \frac{9}{4}a^2 \left[k_x^2 + \frac{q_\nu^2}{3a^2} \right]} \right) \quad (70)$$

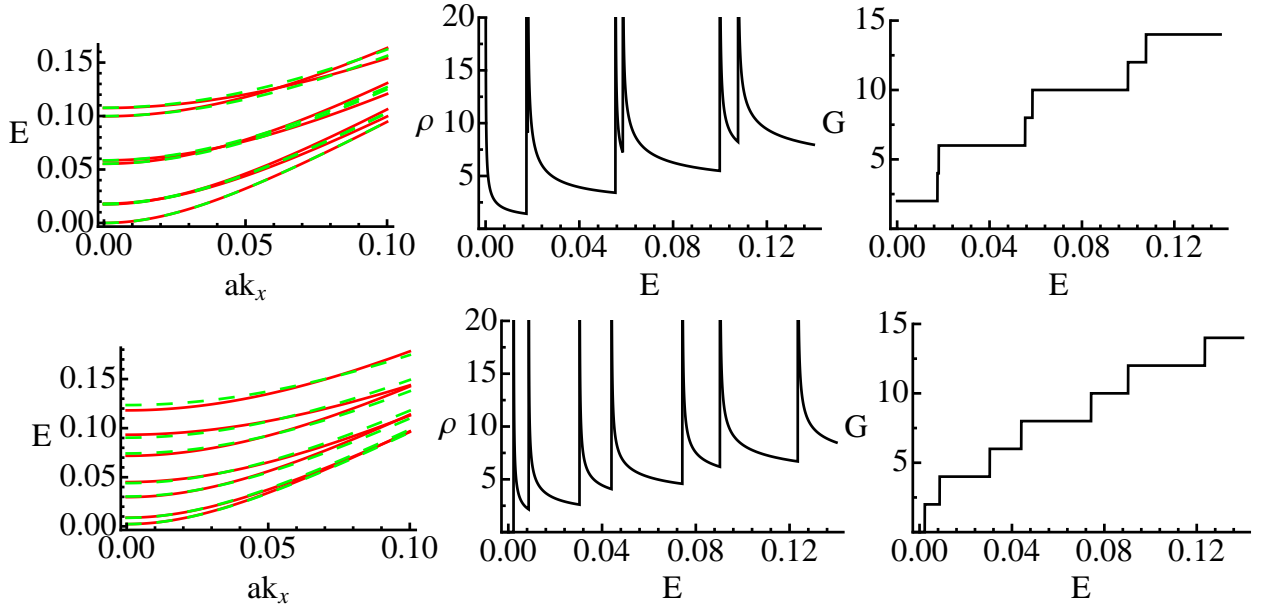


FIG. 6. (Color online) Upper part: band structure of metallic zigzag bilayer carbon tubes (left), DOS (center) and conductance (right). The number of hexagons in the y direction $\mathcal{N} = 102$. Lower part: band structure of semiconducting zigzag bilayer carbon tubes (left), DOS (center) and conductance (right). The number of hexagons in the y direction $\mathcal{N} = 100$. Solid red lines are calculated according Eqs. (44), (45); dashed green lines represent approximation (70). Bands with $s_2 = +1$ are not shown. DOS is given in units of a^{-1} and is calculated according to Eqs. (63), (71). The conductance is given in units of $2e^2/h$ and is calculated using Eq. (61).

Conduction (valence) band bottoms (tops) are equal to

$$E_\nu = s_1 \left(-\frac{\gamma}{2} + \sqrt{\frac{\gamma^2}{4} + \frac{3}{4}q_\nu^2} \right) \quad (71)$$

The number ν of subbands with the index $s_2 = -1$ and energy smaller than the energies of the subbands with index $s_2 = +1$ is greater than 1 only when the number of hexagons in the y direction \mathcal{N} is sufficiently large. Approximating Eq. (71) as $3\pi^2\nu^2/(\gamma\mathcal{N}^2)$ we get $\mathcal{N} \gg \sqrt{3}\pi/\gamma$. In calculations we used $\mathcal{N} = 102$ for metallic tubes and $\mathcal{N} = 100$ for semiconducting tubes.

The band structure, calculated with the use of exact Eqs. (44), (45) and approximated according to Eq. (70) for metallic and for semiconducting tubes is shown in Fig. 6. One sees that Eq. (70) provides accurate reproduction of exact results. Also is shown the DOS, calculated with Eqs. (63), (71), and the conductance $G(E) = (2e^2/h)2n$.

E. Armchair bilayer graphene ribbon

For the armchair bilayer graphene ribbon with AB- α stacking, the condition for the wave-vector component ξ has a simple expression. When $V = 0$ and $j^* \equiv 2(\mathcal{N} + 1)/3$ is an integer then the armchair bilayer graphene ribbon is metallic. Then index $\nu = j - j^* = 0$ corresponds to the zero-energy band. If $2(\mathcal{N} + 1)/3$ is not an integer, armchair bilayer graphene ribbon spectrum has a gap, and the band closest to zero is either $j^* \equiv (2\mathcal{N} + 1)/3$ or $j^* \equiv (2\mathcal{N} + 3)/3$ depending on which of these two numbers is an integer. For $\kappa, \nu/\mathcal{N} \ll 1$ we get Eq. (69) with

$$q_\nu = \begin{cases} \frac{\pi}{\mathcal{N}+1} \left| \nu - \frac{1}{3} \right| \ll 1, & \text{semiconducting} \\ \frac{\pi|\nu|}{\mathcal{N}+1} \left(1 + \frac{\pi\nu}{4\sqrt{3}(\mathcal{N}+1)} \right) \ll 1, & \text{metallic} \end{cases} \quad (72)$$

with $\nu = 0, \pm 1, \dots$. The wave vector component κ is continuous. The difference between the boundary conditions for armchair bilayer graphene ribbons and zigzag bilayer graphene tubes results in about two-times smaller band spacing in the armchair ribbon spectrum than it was found for the zigzag tube spectrum.

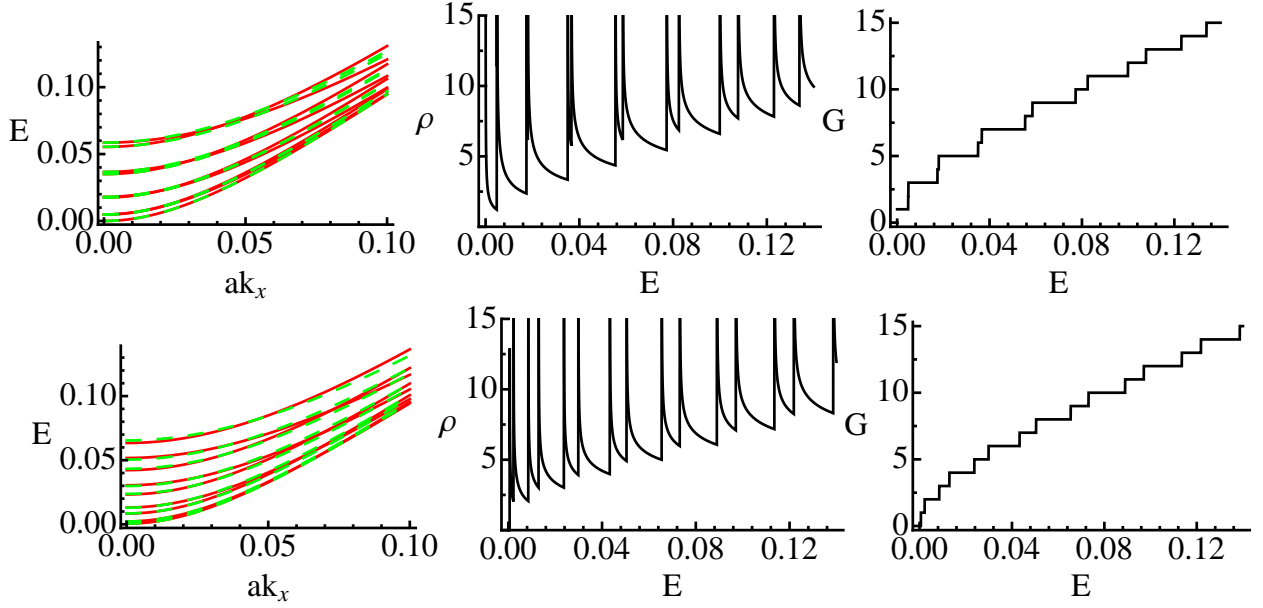


FIG. 7. (Color online) Upper part: band structure of metallic armchair bilayer graphene ribbon with AB- α stacking (left), DOS (center) and conductance (right). The number of hexagons in the y direction $\mathcal{N} = 101$. Lower part: band structure of semiconducting armchair bilayer graphene ribbon with AB- α stacking (left), DOS (center) and conductance (right). The number of hexagons in the y direction $\mathcal{N} = 100$. Solid red lines are calculated according Eqs. (44), (45); dashed green lines represent approximation (73). Bands with $s_2 = +1$ are not shown. DOS is given in units of a^{-1} and is calculated according to Eqs. (63), (74). The conductance is given in units of $2e^2/h$ and is calculated using Eq. (61).

The energy spectrum has the form

$$E_\nu(k_x) = s_1 \left(-\frac{\gamma}{2} + \sqrt{\frac{\gamma^2}{4} + \frac{9}{4}a^2 \left[k_x^2 + \frac{q_\nu^2}{3a^2} \right]} \right) \quad (73)$$

Conduction (valence) band bottoms (tops) are equal to

$$E_\nu = s_1 \left(-\frac{\gamma}{2} + \sqrt{\frac{\gamma^2}{4} + \frac{3}{4}q_\nu^2} \right) \quad (74)$$

The number ν of subbands with the index $s_2 = -1$ and energy smaller than the energies of the subbands with index $s_2 = +1$ is greater than 1 only when the number of hexagons in the y direction \mathcal{N} is sufficiently large. Approximating Eq. (74) as $3\pi^2\nu^2/(4\gamma(\mathcal{N}+1)^2)$ we get $\mathcal{N} \gg \sqrt{3\pi}/(2\gamma)$. In calculations we used $\mathcal{N} = 101$ for metallic ribbons and $\mathcal{N} = 100$ for semiconducting ribbons.

The band structure, calculated with the use of exact Eqs. (44), (45) and approximated according to Eq. (73) for metallic and semiconducting ribbons is shown in Fig. 7. One sees that Eq. (73) provides accurate reproduction of exact results. Also is shown the DOS, calculated with Eqs. (63), (74), and the conductance $G(E) = (2e^2/h)n$.

For the armchair bilayer graphene ribbon with AB- β stacking there are no explicit expressions for the possible values of q .

F. Zigzag bilayer graphene ribbon

In zigzag bilayer graphene ribbons the wave vector component q is continuous while the possible values of κ are given by the solutions of the equations (49) and (B1), (B2) for AB- α stacking or Eq. (B5) for AB- β stacking, presented in Appendix B. Since equations for κ depend on the value of the wave vector ξ , in zigzag bilayer graphene ribbons longitudinal and transverse motions are not separable. When the energy of the subband with the index $s_2 = -1$ is smaller than the energies of the subbands with index $s_2 = +1$, only one of wave vectors $\kappa^{(1)}$ and $\kappa^{(2)}$ is real valued. Therefore, the energy subbands can be labeled by the value of $\kappa^{(1)} \equiv \kappa_\nu$ only.

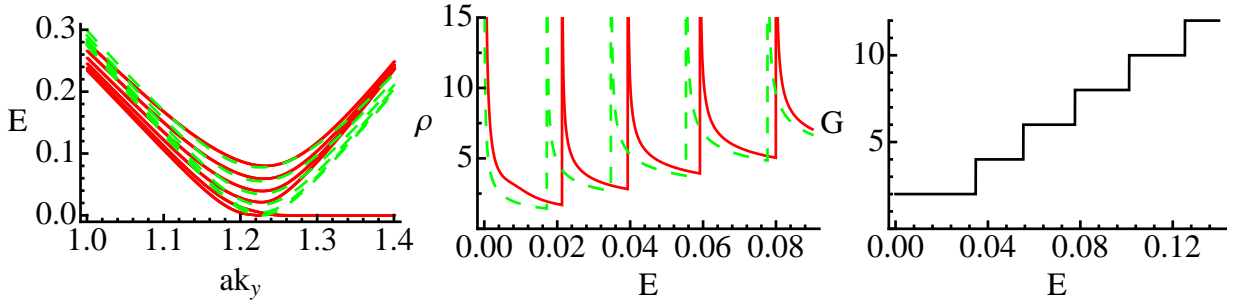


FIG. 8. (Color online) Band structure of zigzag bilayer graphene ribbon with AB- α stacking (left), DOS (center) and conductance (right). The number of rectangular unit cells in the x direction $N = 60$. Solid red lines are calculated according Eqs. (44), (45) with the allowed values of the wave vector κ obtained solving Eqs. (B1), (B2) and (49); dashed green lines represent approximation (75). Bands with $s_2 = +1$ are not shown. DOS is given in units of a^{-1} . The conductance is given in units of $2e^2/h$ and is calculated using Eq. (61).

Depending on the value of $|\xi|$, wave vectors κ_ν with $\nu = 0, 1$ can become imaginary. There are two critical values $\xi^{c(1)}, \xi^{c(2)}$ ($\xi^{c(1)} < \xi^{c(2)}$) of the wave vector ξ , obtained by solving Eqs. (49) and (B1), (B2) or (B5) with $\kappa^{(1)} = 0$. When $\xi^{c(1)} < |\xi| < \xi^{c(2)}$ then one solution κ_0 becomes imaginary whereas in the case $\xi^{c(2)} < |\xi|$ two solutions κ_0 and κ_1 become imaginary. Both critical values $\xi^{c(1,2)}$ obey the inequality $\xi^{c(1,2)} > 2\pi/3$ and tend to the limit $2\pi/3$ as the number N grows. More tight lower bound of critical values is $\xi^{c(1,2)} > 2 \arccos[N/(2N+1)]$. The imaginary solutions κ_ν represent edge states in zigzag bilayer graphene ribbons.

The energy bands of bilayer graphene are asymmetric near the point $q = 0$. The subbands (except corresponding to edge states) can be approximated by taking $\kappa_\nu \approx \pi\nu/N$ and the minimum of of the subband located at $\xi^{c(2)}$:

$$E_\nu(k_y) = s_1 \left(-\frac{\gamma}{2} + \sqrt{\frac{\gamma^2}{4} + \frac{9}{4}a^2 \left[(k_y - \bar{k}_y)^2 + \frac{\pi^2\nu^2}{9a^2N^2} \right]} \right) \quad (75)$$

with

$$\bar{k}_y = \frac{\xi^{c(2)}}{\sqrt{3}a}. \quad (76)$$

The critical value $\xi^{c(2)}$ of the wave vector tends to the limit $2\pi/3$ as the number N grows. Conduction (valence) band bottoms (tops) are equal to

$$E_\nu = s_1 \left(-\frac{\gamma}{2} + \sqrt{\frac{\gamma^2}{4} + \frac{\pi^2\nu^2}{4N^2}} \right) \quad (77)$$

The number ν of of subbands with the index $s_2 = -1$ and energy smaller than the energies of the subbands with index $s_2 = +1$ is greater than 1 only when the number of rectangular unit cells in the x direction N is sufficiently large. Approximating Eq. (77) as $\pi^2\nu^2/(4\gamma N^2)$ we get $N \gg \pi/(2\gamma)$. In calculations we used $N = 60$.

The band structure for zigzag bilayer graphene ribbons with AB- α stacking, calculated with the use of exact Eqs. (44), (45) with the allowed values of the wave vector κ obtained solving Eqs. (B1), (B2) and (49), as well as approximation (75) are represented in Fig. 8. Also is shown the DOS and the conductance $G(E) = (2e^2/h)(2n+2)$. The DOS is calculated from exact band structure and also using Eqs. (63), (74), taking the threshold energies for $\nu = 0, 1$ to be $E_{\nu=0,1} = 0$. The band structure of zigzag bilayer graphene ribbons with AB- β stacking is very similar to the band structure of ribbons with AB- α stacking, only the critical values $\xi^{c(1)}, \xi^{c(2)}$ are slightly different.

Taking the limit $N \rightarrow \infty$ in the zigzag bilayer graphene ribbon with AB- β stacking one can obtain the edge states of Ref. 29. However, care should be taken not to loose any solutions. For large number N we can write the absolute value of the imaginary wave vector $i|\kappa|$ as $|\kappa| = \kappa^{(0)} + \delta$, where $\kappa^{(0)}$ is the solution of the equation

$$e^{-\frac{\kappa^{(0)}}{2}} = 2 \cos(\xi/2) \quad (78)$$

and δ is a small correction. From Eq. (44) it follows that such a value of $\kappa^{(0)}$ ensures the equality $E(i\kappa^{(0)}, \xi) = 0$. Expanding Eq. (44) in powers of δ we get the approximate expression for the energy

$$E \approx \frac{s_1\delta}{\gamma} \left(2 \cos^2 \left(\frac{\xi}{2} \right) - \frac{1}{2} \right). \quad (79)$$

There are two eigenstates with wave vectors $\kappa^{(1)}$ and $\kappa^{(2)}$ having different absolute values but corresponding the same energy. From Eqs. (79) and (48) it follows that the corrections to the wave vector obey the condition

$$\delta^{(2)} = -\delta^{(1)}. \quad (80)$$

In Eq. (B5) taking into account only the first-order terms with respect to δ one obtains the value of the correction

$$\delta = \pm 2e^{-2\kappa^{(0)}N}(1 - e^{-\kappa^{(0)}}). \quad (81)$$

This expression for the correction is the same as for the single sheet of graphene. The correction δ decreases exponentially with increasing the number N .

For large N it is sufficient to form the wave function obeying boundary conditions (47) as a superposition of two exponentially decreasing terms with the wave vectors $i|\kappa^{(1)}|$ and $i|\kappa^{(2)}|$,

$$\psi_{m,n,\alpha_p} = a^{(1)}c_{\alpha_p}(\xi_j, i|\kappa^{(1)}|)e^{i\xi_j m - |\kappa^{(1)}|n} + a^{(2)}c_{\alpha_p}(\xi_j, i|\kappa^{(2)}|)e^{i\xi_j m - |\kappa^{(2)}|n}. \quad (82)$$

Substituting this expression for the wave function in the boundary conditions, using Eqs. (A9)–(A12) and taking the limit $N \rightarrow \infty$ we obtain two solutions for the coefficients $a^{(1)}$, $a^{(2)}$: $a^{(2)} = 0$ and $a^{(2)} = -a^{(1)}$. The wave function corresponding to the solution $a^{(2)} = 0$ is localized on the first layer, with the nonzero coefficients c_{l_1} and c_{ρ_1} . The wave function corresponding to the solution $a^{(2)} = -a^{(1)}$ contains the difference $e^{-|\kappa^{(1)}|n} - e^{-|\kappa^{(2)}|n}$. Expanding to the first order of δ we get

$$e^{-|\kappa^{(1)}|n} - e^{-|\kappa^{(2)}|n} = e^{-(\kappa^{(0)} - \delta)n} - e^{-(\kappa^{(0)} + \delta)n} \approx 2\delta n e^{-\kappa^{(0)}n}. \quad (83)$$

Taking the limit $N \rightarrow \infty$ and dropping the coefficients of the wave function that are of the order of δ we obtain that nonzero coefficients are ψ_{m,n,l_1} , ψ_{m,n,ρ_1} in the first layer and ψ_{m,n,r_2} , ψ_{m,n,λ_2} in the second layer. The coefficients ψ_{m,n,r_2} , ψ_{m,n,λ_2} are proportional to $e^{-\kappa^{(0)}n}$ while the coefficients ψ_{m,n,l_1} , ψ_{m,n,ρ_1} have $ne^{-\kappa^{(0)}n}$ behavior, as in Ref. 29.

V. CONCLUSIONS

An exact analytical description of π electron spectrum based on tight-binding model of bilayer graphene has been presented. The bilayer graphene structures considered in this article have rectangular geometry and finite size in one or both directions with armchair- and zigzag-shaped edges. This includes bilayer graphene nanoribbons and nanotubes. The exact solution of the Schrödinger problem, the spectrum and wave functions, has been obtained and used to analyze the density of states and the conductance quantization. Our method brings a connection between π electron spectrum in infinite and finite-size bilayer graphene.

ACKNOWLEDGMENTS

The authors acknowledge a collaborative grant from the Swedish Institute and a grant No. MIP-123/2010 by the Research Council of Lithuania. I.V.Z acknowledges a support from the Swedish Research Council (VR).

Appendix A: Eigenvectors of bilayer graphene using rectangular unit cells

The expressions for the coefficients of the eigenvectors are: For AB- α stacking, $V = 0$

$$c_{r_1} = 1, \quad c_{\rho_1} = -e^{-i\frac{\xi}{2}} \frac{E(\kappa, \xi)}{\phi(-\kappa, \xi)}, \quad (A1)$$

$$c_{l_1} = -s_3 e^{-i\frac{\kappa}{2}} \frac{E(\kappa, \xi)}{\phi(-\kappa, \xi)}, \quad c_{\lambda_1} = s_3 e^{-i\frac{1}{2}(\kappa + \xi)}, \quad (A2)$$

$$c_{r_2} = -s_1 s_2 \frac{\phi(\kappa, \xi)}{\phi(-\kappa, \xi)}, \quad c_{\rho_2} = s_1 s_2 e^{-i\frac{\xi}{2}} \frac{E(\kappa, \xi)}{\phi(-\kappa, \xi)}, \quad (A3)$$

$$c_{l_2} = s_1 s_2 s_3 e^{i\frac{\kappa}{2}} \frac{E(\kappa, \xi)}{\phi(-\kappa, \xi)}, \quad c_{\lambda_2} = -s_1 s_2 s_3 e^{i\frac{1}{2}(\kappa - \xi)} \frac{\phi(\kappa, \xi)}{\phi(-\kappa, \xi)}. \quad (A4)$$

For AB- α stacking, $V \neq 0$

$$c_{r_1} = 1, \quad c_{\rho_1} = -e^{-i\frac{\xi}{2}} \frac{E+V}{\phi(-\kappa, \xi)}, \quad (\text{A5})$$

$$c_{l_1} = -s_3 e^{-i\frac{\kappa}{2}} \frac{E+V}{\phi(-\kappa, \xi)}, \quad c_{\lambda_1} = s_3 e^{-i\frac{1}{2}(\kappa+\xi)}, \quad (\text{A6})$$

$$c_{r_2} = -\frac{\phi(\kappa, \xi)}{\phi(-\kappa, \xi)} f(\kappa, \xi), \quad c_{\rho_2} = s_1 s_2 e^{-i\frac{\xi}{2}} \frac{E-V}{\phi(-\kappa, \xi)} f(\kappa, \xi), \quad (\text{A7})$$

$$c_{l_2} = s_1 e^{i\frac{\kappa}{2}} \frac{E-V}{\phi(-\kappa, \xi)} f(\kappa, \xi), \quad c_{\lambda_2} = -s_3 e^{i\frac{1}{2}(\kappa-\xi)} \frac{\phi(\kappa, \xi)}{\phi(-\kappa, \xi)} f(\kappa, \xi). \quad (\text{A8})$$

For AB- β stacking, $V = 0$

$$c_{r_1} = 1, \quad c_{\rho_1} = -e^{-i\frac{\xi}{2}} \frac{\phi(\kappa, \xi)}{E(\kappa, \xi)}, \quad (\text{A9})$$

$$c_{l_1} = -s_3 e^{-i\frac{\kappa}{2}} \frac{\phi(\kappa, \xi)}{E(\kappa, \xi)}, \quad c_{\lambda_1} = s_3 e^{-i\frac{1}{2}(\kappa+\xi)}, \quad (\text{A10})$$

$$c_{r_2} = -s_1 s_2 s_3 e^{i\frac{1}{2}(\xi-\kappa)}, \quad c_{\rho_2} = s_1 s_2 s_3 e^{-i\frac{\kappa}{2}} \frac{\phi(-\kappa, \xi)}{E(\kappa, \xi)}, \quad (\text{A11})$$

$$c_{l_2} = s_1 s_2 e^{i\frac{\xi}{2}} \frac{\phi(-\kappa, \xi)}{E(\kappa, \xi)}, \quad c_{\lambda_2} = -s_1 s_2. \quad (\text{A12})$$

For AB- β stacking, $V \neq 0$

$$c_{r_1} = 1, \quad c_{\rho_1} = -e^{-i\frac{\xi}{2}} \frac{\phi(\kappa, \xi)}{E+V}, \quad (\text{A13})$$

$$c_{l_1} = -s_3 e^{-i\frac{\kappa}{2}} \frac{\phi(\kappa, \xi)}{E+V}, \quad c_{\lambda_1} = s_3 e^{-i\frac{1}{2}(\kappa+\xi)}, \quad (\text{A14})$$

$$c_{r_2} = -s_3 e^{i\frac{1}{2}(\xi-\kappa)} f(\kappa, \xi), \quad c_{\rho_2} = s_3 e^{-i\frac{\kappa}{2}} \frac{\phi(-\kappa, \xi)}{E-V} f(\kappa, \xi), \quad (\text{A15})$$

$$c_{l_2} = s_1 s_2 e^{i\frac{\xi}{2}} \frac{\phi(-\kappa, \xi)}{E-V} f(\kappa, \xi), \quad c_{\lambda_2} = -f(\kappa, \xi). \quad (\text{A16})$$

Appendix B: Wave vectors of zigzag bilayer carbon tubes

For AB- α stacking and $V = 0$ the possible values of $\kappa_{j,\nu_j}^{(1)}$ are solutions of one of the equations

$$1 + \cos\left(\frac{\xi}{2}\right) \left(s_3^{(1)} \frac{\cos\left(\frac{1}{2}\kappa^{(1)}(N+1)\right)}{\cos\left(\frac{1}{2}\kappa^{(1)}N\right)} + s_3^{(2)} \frac{\sin\left(\frac{1}{2}\kappa^{(2)}(N+1)\right)}{\sin\left(\frac{1}{2}\kappa^{(2)}N\right)} \right) = 0 \quad (\text{B1})$$

or

$$1 + \cos\left(\frac{\xi}{2}\right) \left(s_3^{(1)} \frac{\sin\left(\frac{1}{2}\kappa^{(1)}(N+1)\right)}{\sin\left(\frac{1}{2}\kappa^{(1)}N\right)} + s_3^{(2)} \frac{\cos\left(\frac{1}{2}\kappa^{(2)}(N+1)\right)}{\cos\left(\frac{1}{2}\kappa^{(2)}N\right)} \right) = 0 \quad (\text{B2})$$

When $V \neq 0$ then the equation for κ reads

$$\begin{aligned} & \frac{1}{4} (f(\kappa^{(1)}) - f(\kappa^{(2)}))^2 \left(1 + 2s_3^{(1)} \cos\left(\frac{\xi}{2}\right) \frac{\sin\left(\kappa^{(1)}\left(N + \frac{1}{2}\right)\right)}{\sin(\kappa^{(1)}N)} \right) \left(1 + 2s_3^{(2)} \cos\left(\frac{\xi}{2}\right) \frac{\sin\left(\kappa^{(2)}\left(N + \frac{1}{2}\right)\right)}{\sin(\kappa^{(2)}N)} \right) \\ & - f(\kappa^{(1)})f(\kappa^{(2)}) \cos^2\left(\frac{\xi}{2}\right) \left(s_3^{(1)} \frac{\cos\left(\frac{1}{2}\kappa^{(1)}(N+1)\right)}{\cos\left(\frac{1}{2}\kappa^{(1)}N\right)} - s_3^{(2)} \frac{\cos\left(\frac{1}{2}\kappa^{(2)}(N+1)\right)}{\cos\left(\frac{1}{2}\kappa^{(2)}N\right)} \right) \\ & \quad \times \left(s_3^{(1)} \frac{\sin\left(\frac{1}{2}\kappa^{(1)}(N+1)\right)}{\sin\left(\frac{1}{2}\kappa^{(1)}N\right)} - s_3^{(2)} \frac{\sin\left(\frac{1}{2}\kappa^{(2)}(N+1)\right)}{\sin\left(\frac{1}{2}\kappa^{(2)}N\right)} \right) = 0 \quad (\text{B3}) \end{aligned}$$

Here the function

$$f(\kappa, \xi) = \frac{(E + V)^2 - |\phi(\kappa, \xi)|^2}{\gamma(E - V)} \quad (\text{B4})$$

describes the contribution of the second sheet of graphene to the eigenvector.

For AB- β stacking and $V = 0$ the possible values of κ are solutions of the equation

$$\begin{aligned} & \left(1 + 2s_3^{(1)} \cos\left(\frac{\xi}{2}\right) \frac{\sin\left(\kappa^{(1)}\left(N + \frac{1}{2}\right)\right)}{\sin(\kappa^{(1)}N)} \right) \left(1 + 2s_3^{(2)} \cos\left(\frac{\xi}{2}\right) \frac{\sin\left(\kappa^{(2)}\left(N + \frac{1}{2}\right)\right)}{\sin(\kappa^{(2)}N)} \right) \\ & + \frac{1}{2} s_3^{(1)} s_3^{(2)} \left(\cos\left(\frac{\kappa^{(1)}}{2}\right) \cos\left(\frac{\kappa^{(2)}}{2}\right) + \frac{1 - \cos(\kappa^{(1)}N) \cos(\kappa^{(2)}N)}{\sin(\kappa^{(1)}N) \sin(\kappa^{(2)}N)} \sin\left(\frac{\kappa^{(1)}}{2}\right) \sin\left(\frac{\kappa^{(2)}}{2}\right) \right) - \frac{1}{2} = 0 \end{aligned} \quad (\text{B5})$$

When $V \neq 0$ then the equation for κ is

$$\begin{aligned} & \frac{1}{4} (f(\kappa^{(1)}) - f(\kappa^{(2)}))^2 \left(1 + 2s_3^{(1)} \cos\left(\frac{\xi}{2}\right) \frac{\sin\left(\kappa^{(1)}\left(N + \frac{1}{2}\right)\right)}{\sin(\kappa^{(1)}N)} \right) \left(1 + 2s_3^{(2)} \cos\left(\frac{\xi}{2}\right) \frac{\sin\left(\kappa^{(2)}\left(N + \frac{1}{2}\right)\right)}{\sin(\kappa^{(2)}N)} \right) \\ & + \frac{1}{2} f(\kappa^{(1)}) f(\kappa^{(2)}) \left(1 - s_3^{(1)} s_3^{(2)} \left(\cos\left(\frac{\kappa^{(1)}}{2}\right) \cos\left(\frac{\kappa^{(2)}}{2}\right) \right. \right. \\ & \left. \left. + \frac{1 - \cos(\kappa^{(1)}N) \cos(\kappa^{(2)}N)}{\sin(\kappa^{(1)}N) \sin(\kappa^{(2)}N)} \sin\left(\frac{\kappa^{(1)}}{2}\right) \sin\left(\frac{\kappa^{(2)}}{2}\right) \right) \right) = 0 \end{aligned} \quad (\text{B6})$$

* julius.ruseckas@tfai.vu.lt; <http://www.itpa.lt/~ruseckas>

- ¹ A. H. Castro Neto, F. Guinea, N. M. R. Peres, K. S. Novoselov, and A. K. Geim, *Rev. Mod. Phys.* **81**, 109 (2009).
- ² D. S. L. Abergela, V. Apalkov, J. Berashevich, K. Ziegler, and T. Chakraborty, *Advances in Physics* **59**, 261 (2010).
- ³ S. D. Sarma, S. Adam, E. H. Hwang, and E. Rossi(2010), *Rev. Mod. Phys.*, to be published, arXiv:1003.4731v1 [cond-mat.mes-hall].
- ⁴ N. M. R. Peres, *Rev. Mod. Phys.* **82**, 2673 (2010).
- ⁵ X. Du, I. Skachko, A. Barker, and E. Y. Andrei, *Nature Nanotech* **3**, 491 (2008).
- ⁶ E. McCann, *Phys. Rev. B* **74**, 161403(R) (2006).
- ⁷ J. B. Oostinga, H. B. Heersche, X. Liu, A. F. Morpurgo, and L. M. K. Vandersypen, *Nat. Mat.* **7**, 151 (2007).
- ⁸ F. Xia, D. B. Farmer, Y. Lin, and P. Avouris, *Nano. Lett.* **10**, 715 (2010).
- ⁹ K. Wakabayashi, M. Fujita, H. Ajiki, and M. Sgrist, *Phys. Rev. B* **59**, 8271 (1999).
- ¹⁰ Y.-W. Son, M. L. Cohen, and S. G. Louie, *Phys. Rev. Lett.* **97**, 216803 (2006).
- ¹¹ M. Y. Han, B. Özyilmaz, Y. Zhang, and P. Kim, *Phys. Rev. Lett.* **98**, 206805 (2007).
- ¹² Y.-M. Lin, V. Perebeinos, Z. Chen, and P. Avouris, *Phys. Rev. B* **78**, 161409(R) (2008).
- ¹³ M. Evaldsson, I. V. Zozoulenko, H. Xu, and T. Heinzl, *Phys. Rev. B* **78**, 161407 (2008).
- ¹⁴ E. R. Mucciolo, A. H. Castro Neto, and C. H. Lewenkopf, *Phys. Rev. B* **79**, 075407 (2009).
- ¹⁵ S. Ihnatsenka and G. Kirczenow, *Phys. Rev. B* **80**, 201407 (2009).
- ¹⁶ X. Jia, M. Hofmann, V. Meunier, B. G. Sumpter, J. Campos-Delgado, J. M. Romo-Herrera, H. Son, Y.-P. Hsieh, A. Reina, J. Kong, M. Terrones, and M. S. Dresselhaus, *Science* **323**, 1701 (2009).
- ¹⁷ D. V. Kosynkin, A. L. Higginbotham, A. Sinitskii, J. R. Lomeda, A. Dimiev, B. K. Price, and J. M. Tour, *Nature* **458**, 872 (2009); L. Jiao, L. Zhang, X. Wang, G. Diankov, and H. Dai, *ibid.* **458**, 877 (2009).
- ¹⁸ X. Li, X. Wang, L. Zhang, S. Lee, and H. Dai, *Science* **319**, 1229 (2008).
- ¹⁹ J. Cai, P. Ruffieux, R. Jaafar, M. Bieri, T. Braun, S. Blankenburg, M. Muoth, A. P. Seitsonen, M. Saleh, X. Feng, K. Müllen, and R. Fasel, *Nature* **466**, 470 (2010).
- ²⁰ L. Brey and H. A. Fertig, *Phys. Rev B* **73**, 235411 (2006).
- ²¹ H. Zheng, Z. F. Wang, T. Luo, Q. W. Shi, and J. Chen, *Phys. Rev. B* **75**, 165414 (2007).
- ²² L. Malysheva and A. I. Onipko, *Phys. Rev. Lett.* **100**, 186806 (2008).
- ²³ A. Onipko, *Phys. Rev. B* **78**, 245412 (2008).
- ²⁴ L. Jiang, Y. Zheng, C. Yi, H. Li, and T. Lü, *Phys. Rev. B* **80**, 155454 (2009).
- ²⁵ F. Guinea, A. H. Castro Neto, and N. M. R. Peres, *Phys. Rev. B* **73**, 245426 (2006).
- ²⁶ B. Partoens and F. M. Peeters, *Phys. Rev. B* **74**, 075404 (2006).
- ²⁷ Z. F. Wang, Q. Li, H. Su, X. Wang, Q. W. Shi, J. Chen, J. Yang, and J. G. Hou, *Phys. Rev. B* **75**, 085424 (2007).
- ²⁸ J. Nilsson, A. H. Castro Neto, F. Guinea, and N. M. R. Peres, *Phys. Rev. B* **78**, 045405 (2008).
- ²⁹ E. V. Castro, N. M. R. Peres, J. M. B. Lopes dos Santos, A. H. Castro Neto, and F. Guinea, *Phys. Rev. Lett* **100**, 026802 (2008).

- ³⁰ H. Xu, T. Heinzl, and I. V. Zozoulenko, Phys. Rev. B **80**, 045308 (2009).
- ³¹ H. Xu, T. Heinzl, A. A. Shylau, and I. V. Zozoulenko, Phys. Rev. B **82**, 115311 (2010).
- ³² E. V. Castro, N. M. R. Peres, and J. M. B. Lopes dos Santos, Europhys. Lett. **84**, 17001 (2008).
- ³³ R. Landauer, IBM J. Res. Dev. **1**, 233 (1957); **32**, 306 (1988).
- ³⁴ M. Büttiker, Phys. Rev. Lett. **57**, 1761 (1986).
- ³⁵ M. Büttiker, Phys. Rev. B **38**, 9375 (1988).